IOPscience iopscience.iop.org

Home Search Collections Journals About Contact us My IOPscience

Local field corrections and the influence of exchange and correlation on the microscopic longitudinal dielectric function of copper

This article has been downloaded from IOPscience. Please scroll down to see the full text article.

1990 J. Phys.: Condens. Matter 2 3919

(http://iopscience.iop.org/0953-8984/2/17/003)

View the table of contents for this issue, or go to the journal homepage for more

Download details:
IP Address: 171.66.16.103
The article was downloaded on 11/05/2010 at 05:53

Please note that terms and conditions apply.

J. Phys.: Condens. Matter **2** (1990) 3919–3939. Printed in the UK

Local field corrections and the influence of exchange and correlation on the microscopic longitudinal dielectric function of copper

H Bross, O Belhachemi, B Mekki and A Seoud
Sektion Physik der Universität München, D-8000 München 2,
Federal Republic of Germany

Received 12 June 1989, in final form 16 October 1989

Abstract. Using recent band-structure results obtained in the local-density scheme, the microscopic longitudinal dielectric function for both the diagonal and the non-diagonal elements is evaluated in the random-phase approximation in the energy range up to 2.5 Ryd. In addition, the influence of exchange and correlation is investigated in a self-consistent way within the time-dependent density-functional approach. We have found that the latter may modify the frequency dependence of the real elements of the dielectric matrix by up to 15%, whereas some imaginary elements are changed by up to 40%. In the long-wave limit, the local-field corrections of the macroscopic dielectric function seem to be negligible for most frequencies. For the diagonal elements of the inverse dielectric matrix with non-zero reciprocal lattice vectors, local-field corrections increase the real parts by up to 10% at low frequencies, whereas at higher frequencies their influence is quite small. The imaginary parts are decreased over the whole frequency range by up to 30%. For all spectra, local-field corrections smooth the structures and the inclusion of exchange and correlation decreases the values of the elements of dielectric matrix. In addition, for realistic wavefunctions, the f sum rule turned out to be badly fulfilled. Plausible arguments for this failure are presented.

1. Introduction

In a many-electron system, an external potential $V_{\text{ext}}(\boldsymbol{r}, t)$ is more or less screened by a redistribution of electrons. Formally, this may be described by the inverse microscopic dielectric function defining the screened potential [1, 27, 54]

$$V_{\text{screen}}(\boldsymbol{r}, t) = \int \varepsilon^{-1}(\boldsymbol{r}, \boldsymbol{r}', t - t')V_{\text{ext}}(\boldsymbol{r}', t')\,\mathrm{d}^3r'\,\mathrm{d}t' \tag{1}$$

or its space–time Fourier transform in a crystal

$$V_{\text{screen}}(\boldsymbol{q} + \boldsymbol{K}, \omega) = \sum_{\boldsymbol{K}'} \varepsilon^{-1}(\boldsymbol{q} + \boldsymbol{K}, \boldsymbol{q} + \boldsymbol{K}', \omega)V_{\text{ext}}(\boldsymbol{q} + \boldsymbol{K}', \omega). \tag{2}$$

In equation (2), $\boldsymbol{q}$ is limited to the first Brillouin zone, and $\boldsymbol{K}$ and $\boldsymbol{K}'$ denote reciprocal lattice vectors. The non-diagonal elements $\varepsilon^{-1}(\boldsymbol{q} + \boldsymbol{K}, \boldsymbol{q} + \boldsymbol{K}', \omega)$ describe the so-called local-field corrections [1, 32, 54], e.g. the rapid oscillations in the response of the solid produced by a slowly varying perturbation V_{ext}. The inverse dielectric function is essential for the understanding of the various phenomena in solid state physics [46, 47]. We do not claim that the following list is complete:

0953-8984/90/173919 + 21 $03.50 © 1990 IOP Publishing Ltd

(i) the scattering of electrons by lattice defects;

(ii) the scattering of electrons by phonons which determines not only the electron–phonon interaction but also the force parameters in lattice dynamics;

(iii) typical magnitudes of the many-body theory, e.g. the total energy, the pair-correlation function and the structure function;

(iv) the plasmon-like collective excitations;

(v) the optical parameters.

Up to now, the dielectric function has been evaluated directly within the framework of the Hartree–Fock theory, which approximates the many-body wavefunction for the ground state and the excited states by a sole Slater determinant [46]. A further simplification is possible by neglecting the interaction between electron–hole states. The latter approximation is sometimes called the Hartree approximation. It is generally believed that the so-called random-phase approximation (RPA), which follows from a severe many-body analysis [23, 27, 35], from the use of double-time Green functions [8] or an investigation of the electron–hole propagator [21], gives a far better approach to the dielectric phenomena. These procedures give the microscopic dielectric function in terms of one-electron wavefunctions and one-electron energies. The inverse problem of the dielectric function according to

$$\int \varepsilon^{-1}(\boldsymbol{r}, \boldsymbol{r}'', \omega)\varepsilon(\boldsymbol{r}'', \boldsymbol{r}', \omega)\, \mathrm{d}^3 r'' = \delta(\boldsymbol{r} - \boldsymbol{r}') \tag{3}$$

still remains [26]. As long as the perturbation slowly varies in space, it could be reduced to a simple matrix inversion.

Expressions of the dielectric function, in terms of one-electron magnitudes, may be derived by use of a self-consistent method, as long as only the Coulomb interactions are taken into account. This was first done by Bardeen [5], in order to understand the electron–phonon interaction and later continued by Hone [30] and Bailyn [3].

It is tempting to go beyond the Hartree approximation within the framework of the local-density formalism (LDF) [29, 37]. This scheme allows us to determine self-consistently the charge density ρ_{ind}, produced by a static external potential V_{ext}:

$$\rho_{\mathrm{ind}}(\boldsymbol{r}, 0) = \int [\varepsilon^{-1}(\boldsymbol{r}, \boldsymbol{r}', 0) - \delta(\boldsymbol{r} - \boldsymbol{r}')]V_{\mathrm{ext}}(\boldsymbol{r}', 0)\, \mathrm{d}^3 r'. \tag{4}$$

Conceptually, this treatment is completely different from that applied by Gupta and Sinha [24], who approximated the electron–electron interaction by a Hubbard-type correlation. For dynamical problems the generalisation of equation (4) may be derived by the use of the time-dependent local-density-functional approach (TLDF) [19, 50, 55].

As we shall see in section 2, exchange and correlation have no influence on the diagonal element $\varepsilon(\boldsymbol{q}, \boldsymbol{q}, \omega)$ in the long-wave limit. However, when going over to the inverse dielectric function, corrections are to be expected, owing to the non-diagonal elements $\varepsilon(\boldsymbol{q} + \boldsymbol{K}, \boldsymbol{q} + \boldsymbol{K}', \omega)$. Apart from investigations done by Kubo [38] which were performed in the static case, no quantitative investigations for a real solid are known which allow a definite conclusion as to whether local-field corrections might be important. Owing to the localised character of d electrons, they certainly become more important in noble and transition metals than in free-electron metals. Therefore, we have performed extensive investigations in the case of Cu, for which the electronic structure has been derived by a modification of the APW method [9, 10, 12].

As a by-product, we have found that the f sum rule, tacitly assumed to be valid, is not well satisfied as a consequence of the Coulomb singularity of the potential yielding radial wavefunction behaviour like $P_l(X, Y, Z)[1 + Zr/(l + 1)]$ near the origin. Here Z denotes the nuclear charge and $P_l(X, Y, Z)$ is a harmonic function of degree l. Application of the momentum operator generates a term of kind $P_{l+1}(X, Y, Z)/r$ which does not belong to the function space of the original function. Thus an infinite number of the original functions are necessary to describe the $P_{l+1}(X, Y, Z)/r$ behaviour. In the pseudopotential approximation this problem will not occur as the corresponding term $P_l(X, Y, Z)$ is not present in the original wavefunctions.

This paper is organised as follows: explicit expressions for the dielectric function are derived within the framework of the self-consistent LDF in section 2. Section 3 deals with the accuracy of the matrix elements of the momentum operator evaluated by using realistic wavefunctions. Details of the work, as well as the reliability of some well known sum rules are discussed in sections 4 and 5. Sections 6 and 7 deal with the calculated dielectric matrix, its inverse and the comparison with experimental results. Finally, in section 8 some conclusions with respect to future investigations are given.

2. Self-consistent evaluation of the dielectric function by use of the local-density formalism

The LDF was originally conceived to determine the ground-state properties of a many-body problem. Its extension to dynamical problems, the TLDF approach [19, 50, 55], is not so well founded. It is based on the assumption that a one-particle density ρ exists for any external potential V_{ext}. Then, the variational derivative of ρ with respect to V_{ext} may be considered as the polarisation function

$$\alpha(1, 2) = e^2 \, \delta\rho_{\text{ind}}(1)/\delta V_{\text{ext}}(2). \tag{5}$$

At least, for external potentials slowly varying in time, we may proceed analogously as in the LDF. A set of one-particle functions is defined by the Schrödinger-like equation

$$(|\boldsymbol{p}|^2/2m)\varphi(\boldsymbol{r}) + V_{\text{eff}}(\boldsymbol{r}, t)\varphi(\boldsymbol{r}) = \mathrm{i}\hbar\dot{\varphi}(\boldsymbol{r}) \tag{6}$$

where the effective potential V_{eff} is defined by

$$V_{\text{eff}}(\boldsymbol{r}, t) = V^0(\boldsymbol{r}) + \delta V_{\text{ext}}(\boldsymbol{r}, t) + e^2 \int \frac{\rho(\boldsymbol{r}')}{|\boldsymbol{r} - \boldsymbol{r}'|} \, \mathrm{d}^3 r' + V_{\text{xc}}[\rho(\boldsymbol{r})] \tag{7}$$

and $V^0(\boldsymbol{r})$ is assumed to be the periodic part of the external potential. As usual, V_{xc} is the local approximation for correlation and exchange.

For vanishing $\delta V_{\text{ext}}(\boldsymbol{r}, t)$, equation (6) defines a complete and orthogonal set of eigenfunctions $\langle \boldsymbol{r}|k\rangle$ from which the unperturbed charge density can be evaluated

$$\rho_0(\boldsymbol{r}) = 2 \sum_k \langle k|\boldsymbol{r}\rangle\langle \boldsymbol{r}|k\rangle \Theta(E_{\text{F}} - \varepsilon_k). \tag{8}$$

Correspondingly, the Fermi energy E_{F} is defined by the implicit equation

$$N = 2 \sum_k \Theta(E_{\text{F}} - \varepsilon_k). \tag{9}$$

In equations (8) and (9) the index k denotes both the band index n and the wavevector $\boldsymbol{k}$ which is restricted to the first Brillouin zone.

In order to take into account the time-dependent external potential, we use the first-order Dirac perturbation theory and assume that at $t \to -\infty$ the external potential $V_{\text{ext}}(\boldsymbol{r}, t)$ is adiabatically switched on to

$$\delta V_{\text{ext}}(\boldsymbol{r}, t) = [V_{\text{ext}}(\boldsymbol{r}, \omega) \exp(-\mathrm{i}\omega t) + V^*_{\text{ext}}(\boldsymbol{r}, \omega) \exp(\mathrm{i}\omega t)] \exp(\eta t) \tag{10}$$

where $\eta \to 0^+$.

Owing to the invariance with respect to time translation both $\delta V_{\text{eff}}(\boldsymbol{r}, t)$ and the change $\delta\rho(\boldsymbol{r}, t)$ in the charge density will have the same time-dependence. At any time $-\infty < t < 0$ we can determine the charge density $\rho(\boldsymbol{r}, t)$ by a relation analogous to equation (8) but $\langle \boldsymbol{r}|k\rangle$ is substituted by $\varphi(\boldsymbol{r}, t)$. Up to linear terms in the perturbation, the Fourier transform of the induced charge density reads

$$\rho_{\text{ind}}(\boldsymbol{r}, \omega) = -\sum_{k' \neq k} \Theta(E_{\text{F}} - \varepsilon_k) \times \left(\frac{\langle k|\boldsymbol{r}\rangle\langle \boldsymbol{r}|k'\rangle\langle k'|V_{\text{eff}}(\boldsymbol{r}, \omega)|k\rangle}{\varepsilon_{k'} - \varepsilon_k - \hbar\omega - \mathrm{i}\eta\hbar} + \frac{\langle k|V_{\text{eff}}(\boldsymbol{r}, \omega)|k'\rangle\langle k'|\boldsymbol{r}\rangle\langle \boldsymbol{r}|k\rangle}{\varepsilon_{k'} - \varepsilon_k + \hbar\omega + \mathrm{i}\eta\hbar} \right). \tag{11}$$

Inserting $\rho_{\text{ind}}(\boldsymbol{r}, \omega)$ into the Fourier transform of equation (7) we get an integral equation for the effective potential δV_{eff} which may be formally written in the form

$$\int \varepsilon_{\text{SCF}}(\boldsymbol{r}, \boldsymbol{r}', \omega) V_{\text{eff}}(\boldsymbol{r}', \omega)\, \mathrm{d}^3 r' = V_{\text{ext}}(\boldsymbol{r}, \omega) \tag{12}$$

where the kernel is simply the dielectric function obtained self-consistently

$$\begin{aligned} \varepsilon_{\text{SCF}}(\boldsymbol{r}, \boldsymbol{r}', \omega) = \delta(\boldsymbol{r} - \boldsymbol{r}') &+ \int \mathrm{d}^3 r'' \left(\frac{e^2}{|\boldsymbol{r} - \boldsymbol{r}''|} + \delta(\boldsymbol{r} - \boldsymbol{r}'') \frac{\mathrm{d}V_{\text{xc}}}{\mathrm{d}\rho}[\rho_0(\boldsymbol{r}'')] \right) \\ &\times \sum_{k' \neq k} \Theta(E_{\text{F}} - \varepsilon_k) \left(\frac{\langle k|\boldsymbol{r}''\rangle\langle \boldsymbol{r}''|k'\rangle\langle k'|\boldsymbol{r}'\rangle\langle \boldsymbol{r}'|k\rangle}{\varepsilon_{k'} - \varepsilon_k - \hbar\omega - \mathrm{i}\eta\hbar} \right. \\ &\left. + \frac{\langle k|\boldsymbol{r}'\rangle\langle \boldsymbol{r}'|k'\rangle\langle k'|\boldsymbol{r}''\rangle\langle \boldsymbol{r}''|k\rangle}{\varepsilon_{k'} - \varepsilon_k + \hbar\omega + \mathrm{i}\eta\hbar} \right). \end{aligned} \tag{13}$$

It coincides with the usual expression derived by an extension of the RPA when the terms multiplied by $\mathrm{d}V_{\text{xc}}/\mathrm{d}\rho$ are neglected [1, 27, 54]. The latter terms describe corrections of the dielectric function within the framework of the LDF at least in the limit $\omega \to 0$. In this limit, equation (13) could also be derived with help of the time-independent perturbation theory. For any static external potential the wavefunction $\varphi(\boldsymbol{r})$ of the time-independent version of equation (6) may be expanded in terms of the complete set $\langle \boldsymbol{r}|k\rangle$. Using many-body techniques, the same relation (13) was derived by Weber [53]. To our knowledge, corrections of the dielectric function as given in equation (13) have only been used to achieve faster convergence in self-consistent electronic structure calculations [28]. In the case of the free-electron metals, several workers have used a similar approach to determine the linear response to an external field [20, 40, 44].

The time–space Fourier transform of ε_{SCF} defined by

$$\varepsilon_{SCF}(\boldsymbol{q}, \boldsymbol{q}', \omega) = \frac{1}{V_0} \int \int \varepsilon_{SCF}(\boldsymbol{r}, \boldsymbol{r}', \omega) \exp(-i\boldsymbol{q} \cdot \boldsymbol{r}) \exp(i\boldsymbol{q}' \cdot \boldsymbol{r}') \, d^3r \, d^3r' \tag{14}$$

may be decomposed in the following way:

$$\varepsilon_{SCF}(\boldsymbol{q}, \boldsymbol{q}', \omega) = \delta_{\boldsymbol{q}\boldsymbol{q}'} + [\alpha_H(\boldsymbol{q}, \boldsymbol{q}', \omega) + \alpha_{xc}(\boldsymbol{q}, \boldsymbol{q}', \omega)] \tag{15}$$

whereby the Hartree term of the non-interacting system is given by

$$\alpha_H(\boldsymbol{q}, \boldsymbol{q}', \omega) = \frac{4\pi}{q^2} \frac{e^2}{V_0} \sum_{k' \neq k} \Theta(E_F - \varepsilon_k) \left(\frac{\langle k| \exp(-i\boldsymbol{q} \cdot \boldsymbol{r})|k'\rangle\langle k'| \exp(i\boldsymbol{q}' \cdot \boldsymbol{r}')|k\rangle}{\varepsilon_{k'} - \varepsilon_k - \hbar\omega - i\eta\hbar} \right.$$
$$\left. + \frac{\langle k| \exp(i\boldsymbol{q}' \cdot \boldsymbol{r}')|k'\rangle\langle k'| \exp(-i\boldsymbol{q} \cdot \boldsymbol{r})|k\rangle}{\varepsilon_{k'} - \varepsilon_k + \hbar\omega + i\eta\hbar} \right). \tag{16}$$

Exchange and correlation effects are described by

$$\alpha_{xc}(\boldsymbol{q}, \boldsymbol{q}', \omega) = \frac{1}{V_0} \sum_{k' \neq k} \Theta(E_F - \varepsilon_k)$$
$$\times \left(\frac{\langle k|dV_{xc}/d\rho) \exp(-i\boldsymbol{q} \cdot \boldsymbol{r})|k'\rangle\langle k'| \exp(i\boldsymbol{q}' \cdot \boldsymbol{r}')|k\rangle}{\varepsilon_{k'} - \varepsilon_k - \hbar\omega - i\eta\hbar} \right.$$
$$\left. + \frac{\langle k| \exp(i\boldsymbol{q}' \cdot \boldsymbol{r}')|k'\rangle\langle k'| \exp(-i\boldsymbol{q} \cdot \boldsymbol{r}) (dV_{xc}/d\rho)|k\rangle}{\varepsilon_{k'} - \varepsilon_k + \hbar\omega + i\eta\hbar} \right). \tag{17}$$

The close similarity of both expressions is quite remarkable. Note that in both expressions the energy denominators are the same. As they characterise the same van Hove singularity, the exchange and correlation corrections will not shift the edge structure of ε_{SCF} significantly. As we shall see in the following, the derivative $dV_{xc}/d\rho$ shows slow variation within the atomic polyhedron with the consequence that for small values of $\boldsymbol{q}$ and $\boldsymbol{q}'$ we may approximately write

$$\alpha_{xc}(\boldsymbol{q}, \boldsymbol{q}', \omega) \simeq (q^2/4\pi e^2)(\overline{dV_{xc}}/d\rho)\alpha_H(\boldsymbol{q}, \boldsymbol{q}', \omega) \tag{18}$$

where $\overline{dV_{xc}}/d\rho$ is a suitably defined average of $dV_{xc}/d\rho$ over an atomic polyhedron. The frequency dependence of the dielectric function corrected by exchange and correlation will look quite the same as in the case of the non-interacting system (see figures 6–8).

The above result has another peculiarity. In the long-wave limit, the Coulomb interaction will survive in the expression for $\varepsilon(\boldsymbol{q}, \boldsymbol{q}', \omega)$. Thus the inverse dielectric function of a crystal defined by

$$\sum_{\boldsymbol{K}''} \varepsilon^{-1}(\boldsymbol{q} + \boldsymbol{K}, \boldsymbol{q} + \boldsymbol{K}'', \omega)\varepsilon(\boldsymbol{q} + \boldsymbol{K}'', \boldsymbol{q} + \boldsymbol{K}', \omega) = \delta_{\boldsymbol{K}\boldsymbol{K}'} \tag{19}$$

where $\boldsymbol{q}$ is restricted to the first Brillouin zone and where the sum goes over all reciprocal lattice vectors will be corrected only by exchange and correlation when non-diagonal elements of $\varepsilon(\boldsymbol{q} + \boldsymbol{K}, \boldsymbol{q} + \boldsymbol{K}', \omega)$ are taken into account. Equations (15)–(17) are the basis of the evaluation of the dielectric function, using realistic many-body structure results. The following steps have to be performed.

(i) The matrix elements of the plane-wave operator must be evaluated. Owing to the

periodicity of the Bloch function, the matrix elements $\langle n', \boldsymbol{k}+\boldsymbol{q}+\boldsymbol{K}'|\exp[\mathrm{i}(\boldsymbol{q}+\boldsymbol{K})\cdot\boldsymbol{r}]|n\boldsymbol{k}\rangle$ are non-zero. The reciprocal lattice vector $\boldsymbol{K}'$ guarantees that $\boldsymbol{k}+\boldsymbol{q}+\boldsymbol{K}'$ lies in the first Brillouin zone.

(ii) The occupied states $(n\boldsymbol{k})$ and the complete set of the states $(n'\boldsymbol{k}')$ should be summed.

3. The accuracy of the matrix elements of the momentum operator

Because of the variational character of the APW method, the calculated wavefunctions are much less accurate than the electron energies. This greatly affects the optical matrix elements and it is interesting to check how accurate these might be. In the past, such an analysis was done by Uspenski *et al* [51] on the basis of LMTO wavefunctions.

In the long-wave limit, the matrix elements $\langle n', \boldsymbol{k}+\boldsymbol{q}|\exp(\mathrm{i}\boldsymbol{q}\cdot\boldsymbol{r})|n\boldsymbol{k}\rangle$ are usually expressed by the matrix elements of the momentum operator by use of the $\boldsymbol{k}$–$\boldsymbol{p}$ formalism, which is based on the completeness of the Bloch functions. As the set of functions generated by the usual band-structure calculation is finite†, we cannot expect this property to be well fulfilled. However, a similar identity may be derived from the fact that both $|n\boldsymbol{k}\rangle$ and $|n', \boldsymbol{k}+\boldsymbol{q}\rangle$ are solutions of the Schrödinger equation [41]:

$$\langle n', \boldsymbol{k}+\boldsymbol{q}|\exp(\mathrm{i}\boldsymbol{q}\cdot\boldsymbol{r})|n\boldsymbol{k}\rangle = (\hbar/m) \times \boldsymbol{q}\{\langle n', \boldsymbol{k}+\boldsymbol{q}|\exp(\mathrm{i}\boldsymbol{q}\cdot\boldsymbol{r})\,\boldsymbol{p}|n\boldsymbol{k}\rangle/[\varepsilon_{n',\boldsymbol{k}+\boldsymbol{q}} - \varepsilon_{n\boldsymbol{k}} - (\hbar^2/2m)q^2]\}. \tag{20}$$

Up to the term $(\hbar^2/2m)q^2$ in the denominator the same expression is quoted in [51]. As the right-hand side is still linear in $\boldsymbol{q}$, we may set $\boldsymbol{q}$ equal to zero in all other factors in the case $n' \neq n$. Thus, up to terms linear in $\boldsymbol{q}$ we arrive at

$$\langle n', \boldsymbol{k}+\boldsymbol{q}|\exp(\mathrm{i}\boldsymbol{q}\cdot\boldsymbol{r})|n\boldsymbol{k}\rangle = \begin{cases} 1 & n' = n \\ (\hbar/m)\boldsymbol{q}[\langle n'\boldsymbol{k}|\boldsymbol{p}|n\boldsymbol{k}\rangle/\varepsilon_{n'\boldsymbol{k}} - \varepsilon_{n\boldsymbol{k}}] & n' \neq n \end{cases} \tag{21}$$

and

$$\nabla\varepsilon_{n\boldsymbol{k}} = (\hbar/m)\langle n\boldsymbol{k}|\boldsymbol{p}|n\boldsymbol{k}\rangle. \tag{22}$$

Provided that the state $(n\boldsymbol{k})$ is not degenerate, iteration up to the second order in $\boldsymbol{q}$ gives

$$\frac{\partial^2\varepsilon_{n\boldsymbol{k}}}{\partial k_j\,\partial k_l} = \frac{\hbar^2}{m}\delta_{jl} + 2\frac{\hbar}{m}\left(\frac{\partial}{\partial q_j}\langle n, \boldsymbol{k}+\boldsymbol{q}|\exp(\mathrm{i}\boldsymbol{q}\cdot\boldsymbol{r})\,p_l|n\boldsymbol{k}\rangle\right)_{\boldsymbol{q}=\boldsymbol{0}} = \frac{\hbar^2}{m}\delta_{jl} + 2\frac{\hbar}{m}\int\frac{\partial u^*_{n,\boldsymbol{k}+\boldsymbol{q}}}{\partial q_j}p_l u_{n\boldsymbol{k}}\,\mathrm{d}^3r \tag{23}$$

where $u_{n\boldsymbol{k}}$ is the periodic part of the Bloch function. Only by explicit use of the completeness relation

$$\frac{\partial}{\partial q_j}[\exp(-\mathrm{i}\boldsymbol{q}\cdot\boldsymbol{r})\,|n, \boldsymbol{k}+\boldsymbol{q}\rangle] = \frac{\hbar}{m}\sum_{n'\neq n}|n'\boldsymbol{k}\rangle\frac{\langle n'\boldsymbol{k}|p_j|n\boldsymbol{k}\rangle}{\varepsilon_{n'\boldsymbol{k}} - \varepsilon_{n\boldsymbol{k}}} \tag{24}$$

do we arrive at the f sum rule

$$\frac{\partial^2\varepsilon_{n\boldsymbol{k}}}{\partial k_j\,\partial k_l} = \frac{\hbar^2}{m}\delta_{jl} + 2\frac{\hbar^2}{m^2}\sum_{n'\neq n}\frac{\langle n\boldsymbol{k}|p_j|n'\boldsymbol{k}\rangle\langle n'\boldsymbol{k}|p_l|n\boldsymbol{k}\rangle}{\varepsilon_{n\boldsymbol{k}} - \varepsilon_{n'\boldsymbol{k}}}. \tag{25}$$

From this consideration we must conclude that only the diagonal matrix elements of the

† The MAPW formalism described later, gives up to 100 Bloch functions for a certain value of $\boldsymbol{k}$.

momentum operator may be checked directly by using equation (22). For that purpose, it is essential that the gradient of the energy may be obtained with the same accuracy as the energy itself, either by numerical differentiation or directly from band-structure calculations. For example, in the case of the MAPW formalism the matrix characterising the general eigenvalue problem is an analytic function of the wavevector. In principle, numerical values of the second derivative $\partial^2 \varepsilon_{nk}/(\partial k_i\, \partial k_j)$ may also be found with slightly less accuracy. We believe that equation (25) is a more severe test of whether the summation over n' includes a sufficient number of bands than for the accuracy of the non-diagonal matrix elements. The same is true for the criterion based on the expectation value of the kinetic energy in the Bloch state:

$$\left\langle nk \left| \frac{|\boldsymbol{p}|^2}{2m} \right| nk \right\rangle = \sum_{j=1}^{3} \sum_{n'} \langle nk|p_j|n'k\rangle\langle n'k|p_j|nk\rangle. \tag{26}$$

On the other hand, tests based on equations (25) and (26) shed some light on the question of how reliable the evaluation of the dielectric function using equation (15), which is also based on the completeness of the Bloch functions, might be. Certainly, equation (20) is a far better starting point for the test of the accuracy of the non-diagonal elements of the momentum operator as it gives

$$\langle n'k|p_j|nk\rangle = (m/\hbar)(\varepsilon_{n'k} - \varepsilon_{nk})(\partial/\partial q_j)(\langle n', k+q| \exp(\mathrm{i}q \cdot r)|nk\rangle)_{q=0}. \tag{27}$$

4. Details of the numerical work

4.1. Band-structure calculation

The wavefunctions $|nk\rangle$ and the energies ε_{nk} have been evaluated by the MAPW formalism [9, 10, 12], using a self-consistent potential derived by two of the present authors [16]. These investigations are quite analogous to those applied in the case of Al [14] or Li [15] and have been done for a warped-muffin-tin potential neglecting multipole moments. For each angular momentum $0 \leq l \leq 2$, we have used four different radial functions $R_{nl}(r)$ which are chosen in such a way that the logarithmic derivative is either $+1$ or -1. All plane waves with

$$|k+K|^2 \leq 15.0(2\pi/a)^2 \tag{28}$$

are considered. Depending on the value of the k-vector, 70–75 different bands have been obtained covering an energy range up to 10 Ryd above the Fermi level. All these bands are taken into account in the following investigations. In contrast, Kubo [38] has considered only 11 different bands. Exchange and correlation effects have been taken into account by using the empirical formula proposed by van Barth and Hedin [52] with parameters taken from Moruzzi *et al* [43]. For details we refer to the work to be published by two of the present authors [16].

According to equation (17), exchange and correlation corrections of the dielectric function depend strongly on the function $\mathrm{d}V_{\mathrm{xc}}/\mathrm{d}\rho$. Figure 1 shows its dominant spherical contribution within the APW sphere. From this curve, we learn that $\mathrm{d}V_{\mathrm{xc}}/\mathrm{d}\rho$ is weakly r dependent. Its magnitude may roughly be approximated by

$$\overline{\frac{\mathrm{d}V_{\mathrm{xc}}}{\mathrm{d}\rho}} = \frac{3}{r_{\mathrm{APW}}^3} \int_0^{r_{\mathrm{APW}}} \frac{\mathrm{d}V_{\mathrm{xc}}}{\mathrm{d}\rho} r^2\, \mathrm{d}r = -4.3832 \text{ au} \tag{29}$$

and causes α_{xc} to be opposite in sign to α_{H}. Thus, these many-body corrections reduce the magnitude of the dielectric function $\varepsilon(q, q', \omega)$ with increasing value of $|q|$.

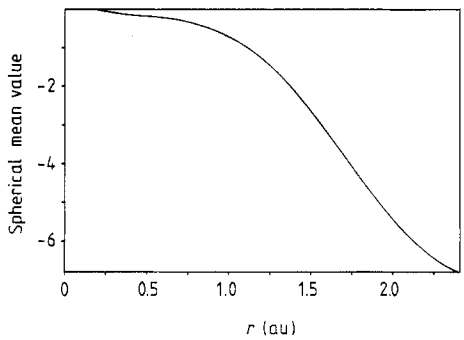

Figure 1. The spherical mean value of the derivative of the exchange and correlation potential with respect to density as a function of r (au).

4.2. Matrix elements

Within the framework of the MAPW scheme, the explicit expression for the matrix elements $\langle n'\boldsymbol{k}|\boldsymbol{p}|n\boldsymbol{k}\rangle$ and $\langle n', \boldsymbol{k}+\boldsymbol{q}|\exp[\mathrm{i}(\boldsymbol{q}+\boldsymbol{K})\cdot\boldsymbol{r}]|n\boldsymbol{k}\rangle$ are quite lengthy and are presented elsewhere [7, 41, 48]. As these expressions consist of only finite sums, they may be evaluated with any accuracy wanted. Thus, only systematic errors occur which are a consequence of the fact that the MAPW formalism solves the Schrödinger equation by a finite Ritz *ansatz*. By the way, we would like to mention one peculiarity of the MAPW formalism. As it yields wavefunctions, which, as well as their first derivatives, are continuous everywhere in the atomic polyhedron, the matrix elements $\langle n'\boldsymbol{k}|\boldsymbol{p}|n\boldsymbol{k}\rangle$ are exactly Hermitian. In the case of the APW scheme [49] or KKR scheme [36] this property could be achieved only by assuming specifically chosen surface terms. In this respect the expression for the matrix elements given by Chen [18] is deficient. For the LMTO method such corrections have already been proposed [39].

4.3. Integration procedures

Similar to a former paper [13], the Brillouin zone was divided in small cubes with the length $(1/M)(2\pi/a)$. The centres of these cubes were chosen to be magic points [4, 17, 42]. All slowly varying functions, e.g. the matrix elements, are approximated by their values at the cube's middle point $\boldsymbol{k}_i$. Inside each cube the arguments of the Heaviside and the delta functions are expanded in terms of the deviation $\boldsymbol{k}-\boldsymbol{k}_i$. Special routines were developed for evaluating the remaining integral [13, 41]. The final evaluations have been done for $M=4$ yielding ten different $\boldsymbol{k}$-points in the irreducible wedge.

5. Accuracy of the numerical procedure

Most of the following tests have been performed for the wavevector $\boldsymbol{k}=(2\pi/a)(0.75, 0.25, 0.25)$.

5.1. Diagonal matrix elements of the momentum operator

For the occupied d bands and the other valence bands with energy up to 5 Ryd above the Fermi energy, the deviations from the corresponding values of $\nabla\varepsilon_{n\boldsymbol{k}}$ are less than 2%. The absolute deviations for the 3s and 3p states are found to be of the same order

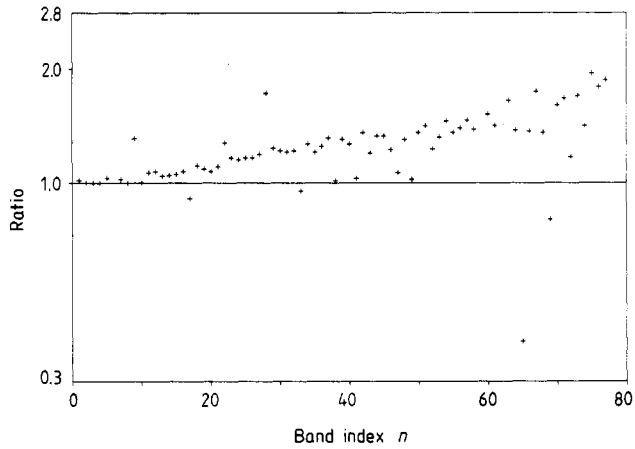

Figure 2. Test of the non-diagonal matrix elements of the momentum operator: the ratio $\langle nk'\boldsymbol{k}|p_j|nk\rangle/(m/\hbar)(\varepsilon_{n'k}-\varepsilon_{nk})(\partial/\partial q_j)(\langle n', \boldsymbol{k}+\boldsymbol{q}|\exp(i\boldsymbol{q}\cdot\boldsymbol{r})|nk\rangle)_{q=0}$ for the band $n'=6$ and $\boldsymbol{k}=(2\pi/\alpha)$ (0.55, 0.45, 0.25) versus the band index n.

as the latter states but, as these matrix elements are two orders of magnitude smaller than those of the valence bands, the relative error is quite large. For the bands with energies more than 5 Ryd above the Fermi level, the Ritz *ansatz* in general badly approximates the wavefunctions. The consequence is that the relative error may reach 100% but, for some states which are almost plane wave like, quite close agreement has been found. Then, both $|nk\rangle$ and $\boldsymbol{p}|nk\rangle$ are well approximated by a superposition of plane waves.

In comparison with the test given in [51], we can conclude that the MAPW formalism yields the diagonal elements of the momentum operator with a considerably higher accuracy than the LMTO formalism does. This is certainly because, firstly, the MAPW functions are continuous everywhere in the atomic polyhedron and, secondly, our Ritz *ansatz* is more flexible.

5.2. Non-diagonal matrix elements of the momentum operator

A test based on equation (27) needs knowledge of the $\boldsymbol{k}$-derivative of the periodic part of the Bloch function which may be obtained from the MAPW eigenvalue problem, too. Figure 2 shows equation (27) for $\boldsymbol{q}$ along the z direction, for the band $n'=6$ and $\boldsymbol{k}=(2\pi/a)(0.55, 0.45, 0.25)$ for all bands produced by the MAPW formalism. For most bands the relative error is of magnitude 20%, with the tendency that it becomes larger at higher bands. These results do not support the supposition quoted in [51] that the non-diagonal elements are of the same accuracy as the diagonal ones.

In figure 3 we want to illustrate that the validity of the f sum rule is based on the number of the excited states considered. For the 3p core band, as well as for the first and third valence band, and $\boldsymbol{k}=(2\pi/a)(0.75, 0.25, 0.25)$, the sum

$$\sigma=\sum_{n'\neq n}^{N_{\max}}\frac{|\langle nk|p_x|n'k\rangle|^2}{\varepsilon_{nk}-\varepsilon_{n'k}} \tag{30}$$

as a function of the upper limit $N_{\max}$ is plotted. The broken lines on the right correspond

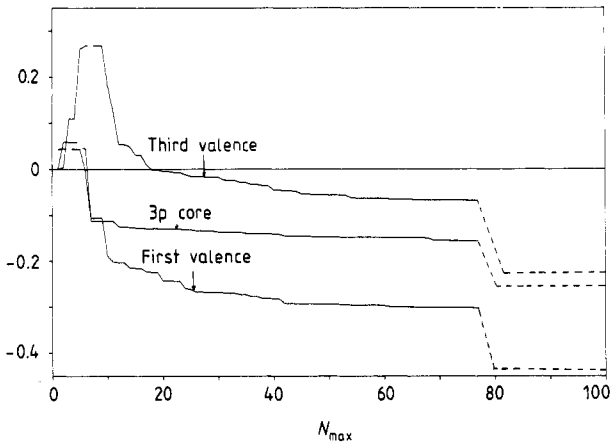

Figure 3. Test of the f sum rule for $\boldsymbol{k} = (2\pi/a)$ (0.75, 0.25, 0.25) and the 3p band, the first and the third valence band. The full curves give equation (30) as a function of the number N_{max} of bands summed over. The broken lines on the right mark the value derived from the second derivative.

to the values derived from the second derivatives. From these results, we must conclude that even by summing up to the eightieth band, the final values are obtained with an error between 30% and 70% depending on the band considered. Similar results are also obtained in the case of the kinetic energy according to equation (26). Because of the poor convergence of the sum over the excited states, both relations turn out to be not suitable to test the validity of the non-diagonal elements of the momentum operator $\boldsymbol{p}$. As a similar sum occurs in the definition of the dielectric function, we expect that it may be evaluated with an error of 20–40%, provided that only 80 excited bands are considered. This result agrees well with the investigations by Ehrenreich and Philipp [22] who found that the oscillator strength for transitions into higher excited states is still distributed for the energy range of 2 Ryd above the Fermi energy.

In order to decide whether the right- or the left-hand side of equation (27) is more accurate, we have also evaluated the sum (30) by substituting $\langle n'\boldsymbol{k}|p_j|n\boldsymbol{k}\rangle$ by $(m/\hbar)(\varepsilon_{n'k} - \varepsilon_{nk})(\partial/\partial_{q_j})\langle n', \boldsymbol{k}+\boldsymbol{q}|\exp(\mathrm{i}\boldsymbol{q}\cdot\boldsymbol{r}|n\boldsymbol{k})\rangle_{q=0}$. In general, this has the result that the f sum rule is slightly better fulfilled. Unfortunately, this way is numerically more complicated and needs higher accuracy.

6. The long-wave limit of the dielectric function

In order to limit the numerical work, the elements of the dielectric function and its inverse have been considered corresponding to reciprocal lattice vectors up to the second shell only. Even then the number of non-zero elements is large but as a consequence of the point group symmetry, which requires that

$$\alpha(\beta(\boldsymbol{q}+\boldsymbol{K}), \beta(\boldsymbol{q}+\boldsymbol{K}'), \omega) = \alpha(\boldsymbol{q}+\boldsymbol{K}, \boldsymbol{q}+\boldsymbol{K}', \omega) \tag{31}$$

is fulfilled for any element β of the point group, there exists a small number of linear independent functions. Similar results also hold for the polarisation functions

$\alpha_H(\boldsymbol{q}+\boldsymbol{K}, \boldsymbol{q}+\boldsymbol{K}', \omega)$, $\alpha_{xc}(\boldsymbol{q}+\boldsymbol{K}, \boldsymbol{q}+\boldsymbol{K}', \omega)$ and the inverse dielectric function $\varepsilon^{-1}(\boldsymbol{q}+\boldsymbol{K}, \boldsymbol{q}+\boldsymbol{K}', \omega)$. In the specific case that one of the reciprocal lattice vectors $\boldsymbol{K}$ or $\boldsymbol{K}'$ is zero, because of equation (31) we may write

$$\alpha(\boldsymbol{q}, \boldsymbol{K}, \omega) = \boldsymbol{q} \cdot \boldsymbol{S}(\boldsymbol{K}, \omega) + O(q^2) \tag{32}$$

in the long-wave limit. The vector functions $\boldsymbol{S}(\boldsymbol{K}, \omega)$ transform as

$$\boldsymbol{S}(\beta\boldsymbol{K}, \omega) = \beta^{-1}\boldsymbol{S}(\boldsymbol{K}, \omega). \tag{33}$$

In a cubic crystal for lattice vectors up to the fourth shell there exists only one scalar function for each shell, such that

$$\boldsymbol{S}(\boldsymbol{K}, \omega) = \boldsymbol{K}\sigma(0, \boldsymbol{K}, \omega). \tag{34}$$

Analogously, we have

$$\alpha(\boldsymbol{q}, \boldsymbol{K}, \omega) = (\boldsymbol{q} \cdot \boldsymbol{K})\sigma(0, \boldsymbol{K}, \omega). \tag{35}$$

As long as we neglect the contribution due to exchange and correlation, the polarisation $\alpha_H(\boldsymbol{q}+\boldsymbol{K}, \boldsymbol{q}+\boldsymbol{K}', \omega)$ as well as the modified dielectric function

$$\chi_H(\boldsymbol{q}+\boldsymbol{K}, \boldsymbol{q}+\boldsymbol{K}', \omega) = (|\boldsymbol{q}+\boldsymbol{K}|/|\boldsymbol{q}+\boldsymbol{K}'|)\alpha_H(\boldsymbol{q}+\boldsymbol{K}, \boldsymbol{q}+\boldsymbol{K}', \omega) \tag{36}$$

are symmetric with respect to $\boldsymbol{K}$ and $\boldsymbol{K}'$.

6.1. The element $\varepsilon(0, 0, \omega)$

The frequency dependence of the leading dielectric function $\varepsilon(0, 0, \omega)$ is shown in figure 4.

In the course of the following discussions, it will become clear that it is reasonable to compare these spectra with the macroscopic dielectric function $\varepsilon(0, \omega)$, which means that, even in the case of noble metals, local-field corrections might be neglected over a wide frequency range. Thus, we have plotted experimental results taken from Hagemann *et al* [25] and from Johnson and Christy [33]. The overall agreement between the theory and experiment on both the magnitude and the location of the structure is quite good, particularly near the interband onset. According to Janak *et al* [31], a stretching of the unoccupied band to higher energies would bring the theoretical curves closer to the experimental curves. Note that, since there is no arbitrary scaling factor in the theory, comparison with the experiment can be made in absolute terms. The interband absorption edge lies at about $\hbar\omega \simeq 0.14$ Ryd. It is encouraging that the calculated amplitudes as well as the shape of the theoretical curve lie quite close to the experimental curves. Some discrepancies may be due to uncertainties in the experimental data or to the means by which measured quantities were extracted, especially Kramers–Kronig inversion of the reflectance data.

The latter uncertainties might be avoided by considering the optical conductivity which is closely related to

$$\sigma(\omega) = (\hbar\omega/4\pi)\varepsilon_2(\omega). \tag{37}$$

Using the multiple-reflection technique, Beaglehole *et al* [6] were able to compute σ without Kramers–Kronig relations. This result is plotted in figure 5 together with the theoretical conductivity spectra (our results and those taken from Uspenski *et al* [51]). Once again the overall correspondence between theory and experiment is satisfactory

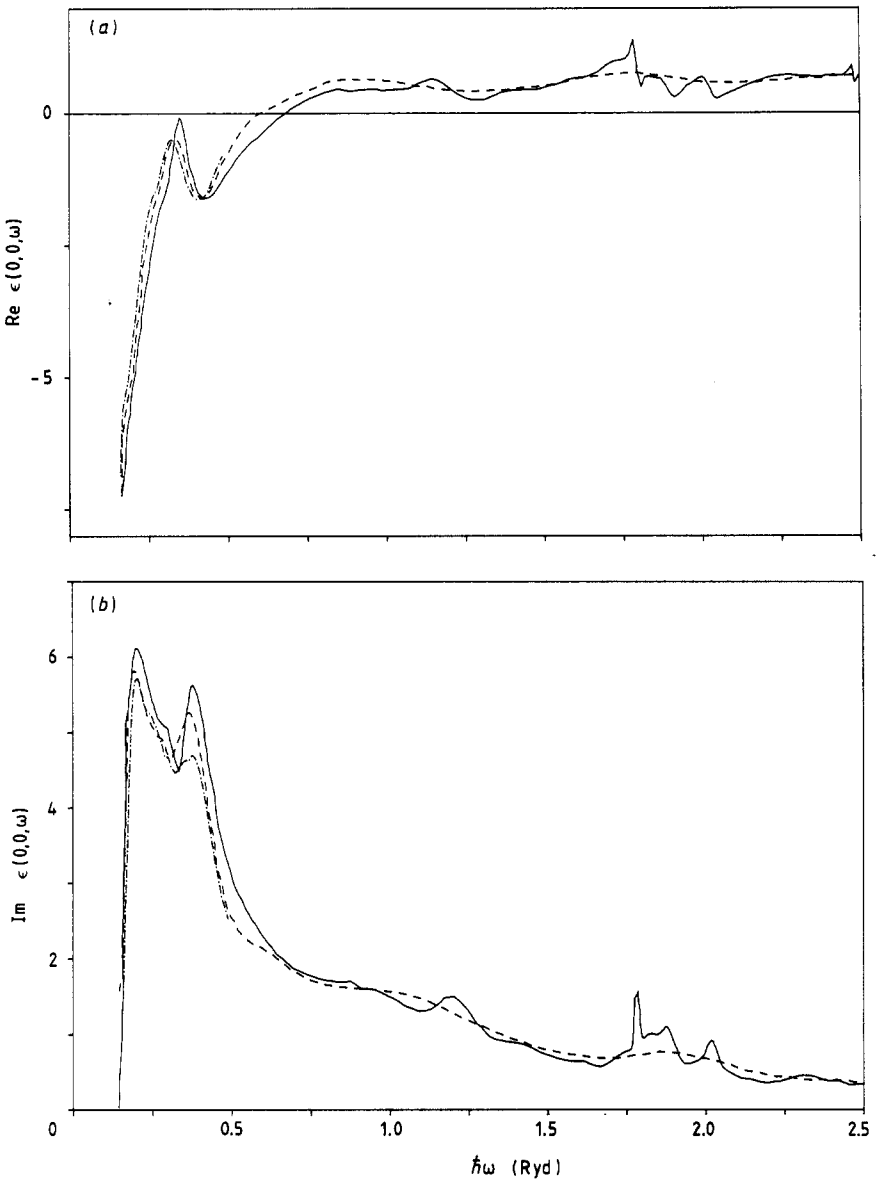

Figure 4. The dependence of the dielectric function $\varepsilon(0, 0, \omega)$ on the energy $\hbar\omega$(Ryd): (*a*) real part; (*b*) imaginary part. The broken curve describes the experimental results taken from [25] and the chain curve those quoted in [33].

in terms of the positions of the main structures and their absolute magnitudes. The hump at 1.20 Ryd corresponds well to the similar broad feature in the experimental curve at 1.07 Ryd. The grouping of structures in the range 1.75–2.0 Ryd is certainly a consequence of the coarse grid used to perform the $\boldsymbol{k}$-integration. Nevertheless, it is conspicuous to assign it to the prominent broad structure in the experimental curve at 1.88 Ryd. Generally speaking, the experimental curves are considerably smoother than

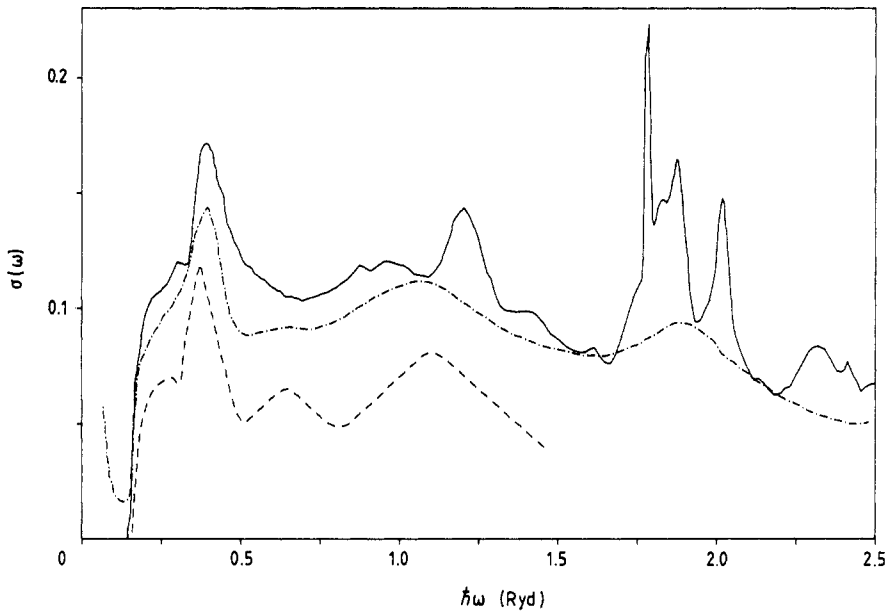

Figure 5. The dependence of the optical conductivity $\sigma(\omega) = (\hbar\omega/4\pi)\varepsilon_2(\omega)$ on the energy $\hbar\omega$(Ryd). The broken curve describes the theoretical results taken from [51] and the chain curve describes the experimental results taken from [6].

the theoretical curves, an effect which can be attributed to the finite lifetime of the final states.

Most of the structure in the theoretical spectra could not uniquely be ascribed to transitions well localised in the Brillouin zone but have their origin in a bunch of transitions covering a large part of k-space. In accordance with [11], the onset of the edge at 0.14 Ryd and the first peak at 0.40 Ryd are due to transitions from the uppermost d band into the hybridised s–p band close to the Fermi level. The broad hump at 1.20 Ryd could be associated with transitions between approximately parallel bands in the neighbourhood of the Σ axis or the X point of the Brillouin zone.

6.2. The elements $\chi(\boldsymbol{K}, \boldsymbol{K}', \omega)$ with at least one non-zero reciprocal lattice vector

In figure 6 the dielectric function $\chi(\boldsymbol{K}, 0, \omega)$ for $\boldsymbol{K} = (2\pi/a)(1, 1, 1)$ is plotted. The full curves show the contribution due only to Coulomb interaction. It coincides completely with the function $\chi(0, \boldsymbol{K}, \omega)$ as in this case the contribution due to exchange is zero. Apart from the fact that these elements of the dielectric matrix are quite small in comparison with $\varepsilon(0, 0, \omega)$, it is only remarkable that the contribution due to exchange is opposite to the direct Coulomb interaction and smooths the frequency dependence considerably.

In the more general case when both reciprocal lattice vectors are non-zero, non-diagonal elements behave completely differently from the diagonal elements. From figure 7 which shows the diagonal elements in the case $\boldsymbol{K} = (2\pi/a)(1, 1, 1)$ we learn that the real part of $\chi(\boldsymbol{K}, \boldsymbol{K}, \omega)$ is quite large and weakly depends on the frequency. The contribution due to exchange seems to be almost constant and tends to lower the value of the real part by 15% and the imaginary part by approximately 40%.

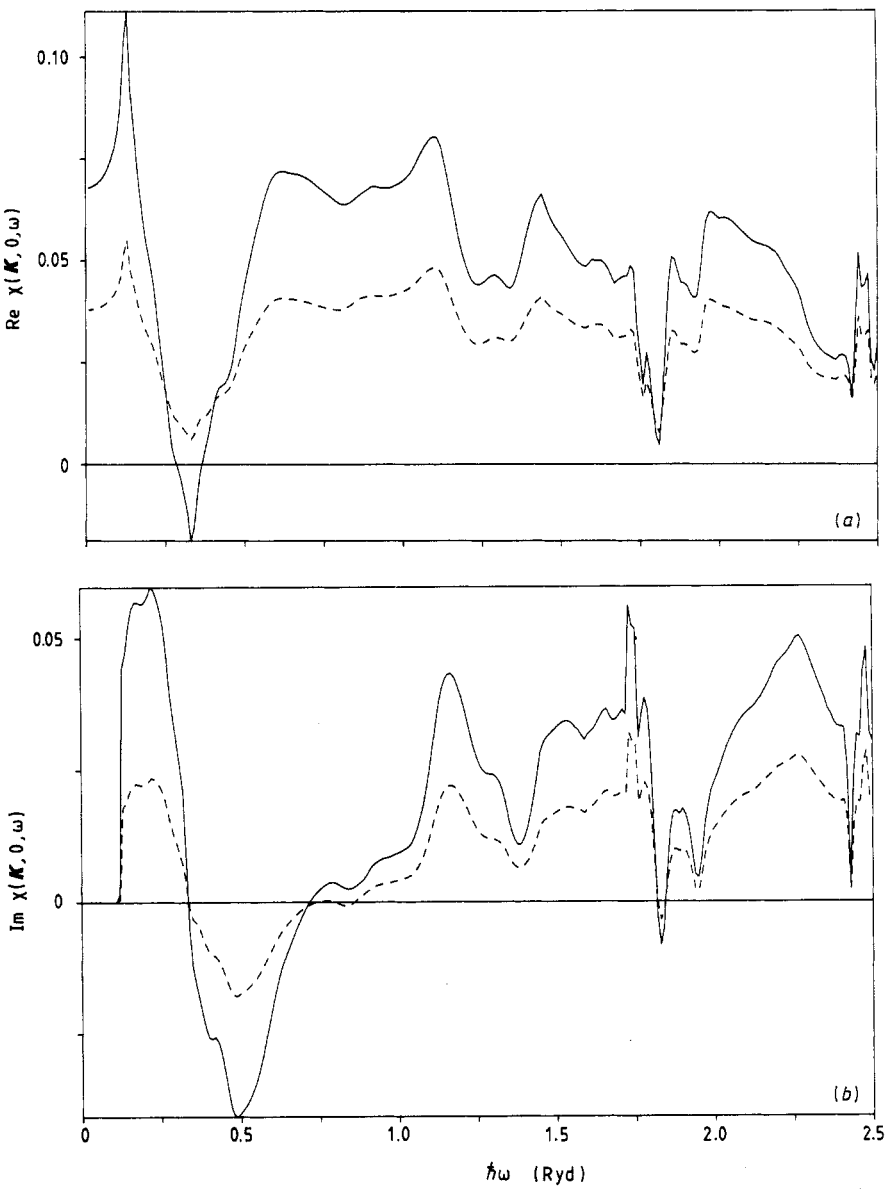

Figure 6. The dependence of the element $\chi(\boldsymbol{K}, 0, \omega)$ on the energy $\hbar\omega$(Ryd) with $\boldsymbol{K} = (2\pi/a)(1, 1, 1)$: (*a*) real part; (*b*) imaginary part. The broken curve incorporates the contribution due to exchange.

In figure 8 a typical example of a non-diagonal element is plotted. All these curves have in common that the real part strongly varies with the frequency and may have different zeros. Its value ranges from -0.1 to 0.2. At $\omega = 1.75$ Ryd a singularity similar to the derivative of a δ-function is to be seen. By a detailed analysis of the contributions coming from different $\boldsymbol{k}$-points we have found that this is attributed to a transition near the point $\boldsymbol{k} = (2\pi/a)(\frac{7}{8}, \frac{1}{8}, \frac{1}{8})$ from the sixth to the fourteenth band. In this case the

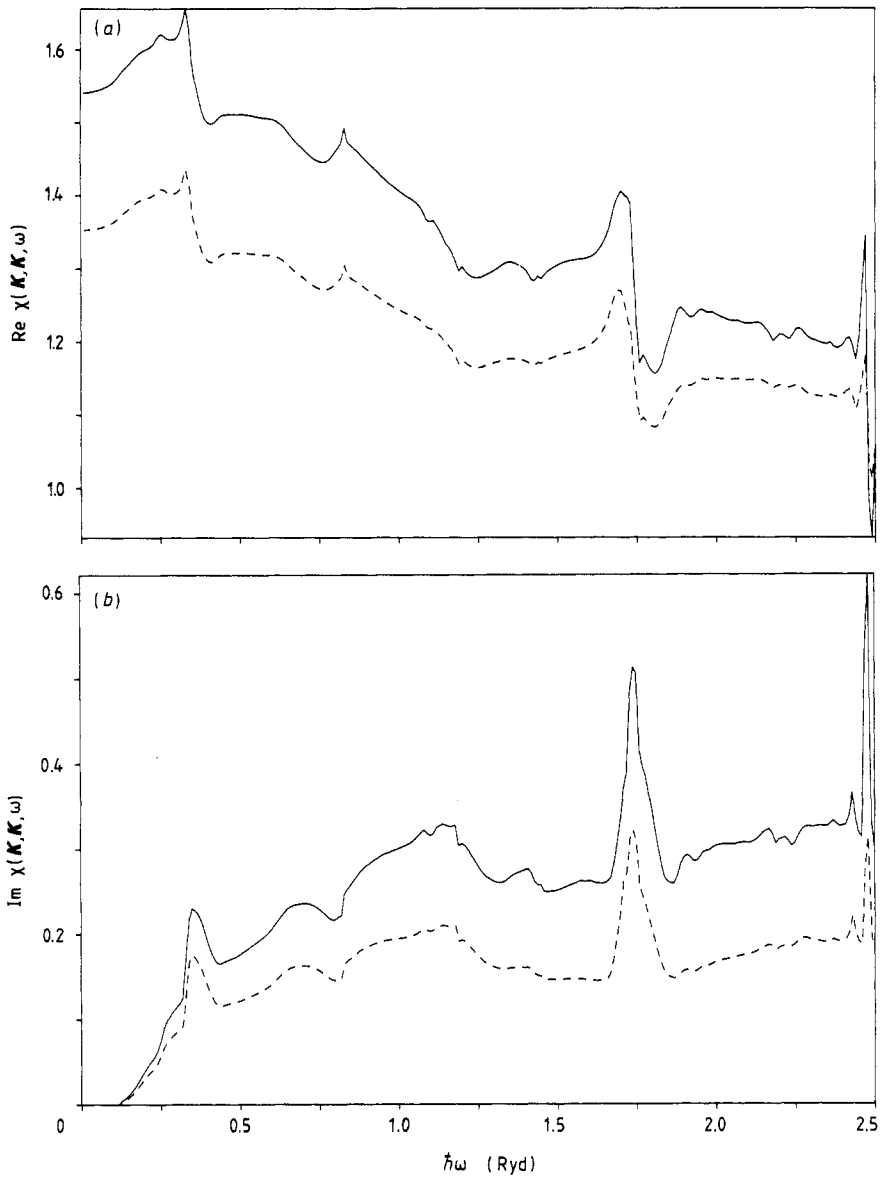

Figure 7. The dependence of the element $\chi(\boldsymbol{K}, \boldsymbol{K}, \omega)$ on the energy $\hbar\omega$(Ryd) with $\boldsymbol{K} = (2\pi/a)$ (1, 1, 1). For further details see figure 6.

contribution due to exchange turns out to be quite small. The imaginary part of the non-diagonal elements is comparable with that of the diagonal elements. Again exchange corrections are quite small and the peak at $\omega = 1.75$ Ryd is present.

7. The long-wave limit of the inverse dielectric function

As long as we restrict ourselves to reciprocal lattice vectors up to the fourth shell, explicit expressions for the inverse dielectric function may be derived by following a procedure

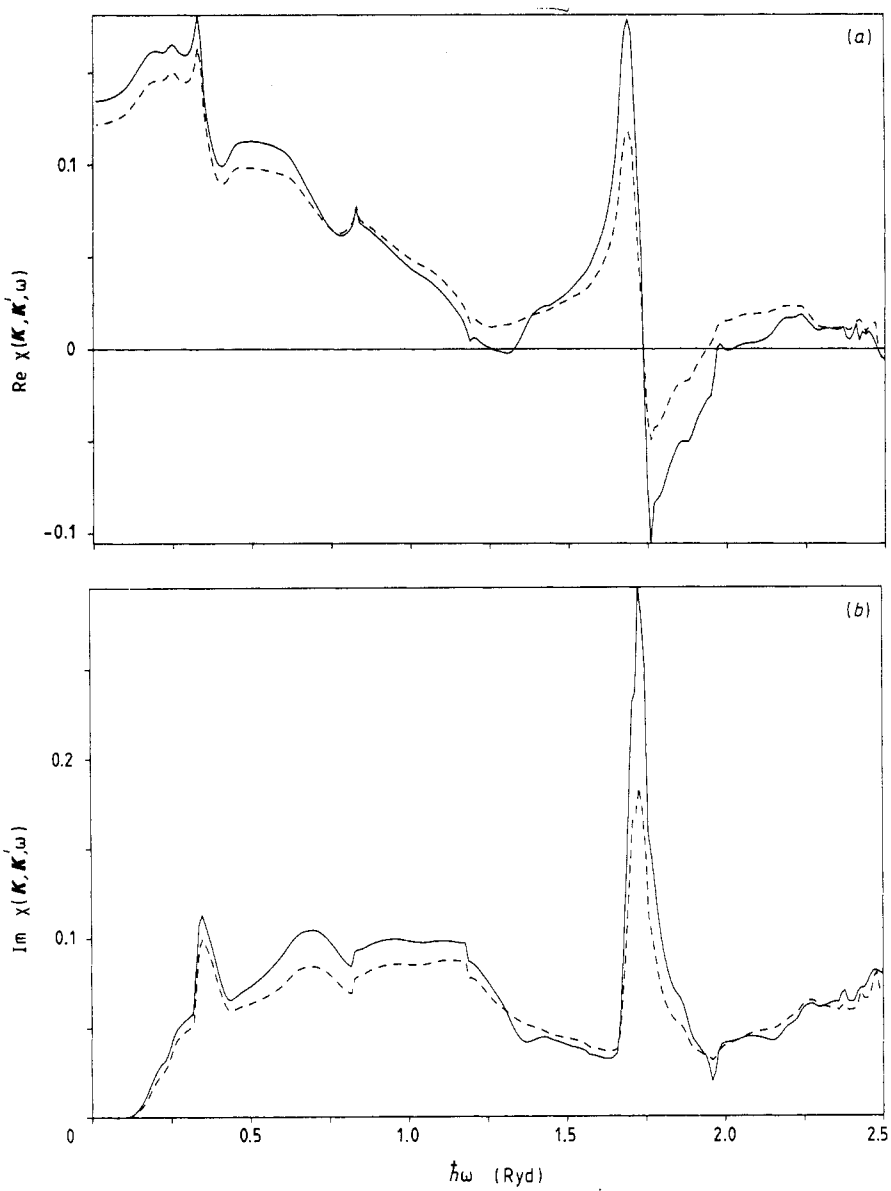

Figure 8. The dependence of the element $\chi(\boldsymbol{K}, \boldsymbol{K}', \omega)$ on the energy $\hbar\omega$(Ryd) with $\boldsymbol{K} = (2\pi/a)\,(2, 0, 0)$ and $\boldsymbol{K}' = (2\pi/a)\,(-2, 0, 0)$. For further details see figure 6.

originally proposed by Pick *et al* [45] and later used by Johnson [32]. For that purpose, we introduce the submatrix $\gamma(\boldsymbol{K}, \boldsymbol{K}', \omega)$ which is the inverse of the lower-right part of the matrix $\chi(\boldsymbol{K}, \boldsymbol{K}', \omega)$ corresponding to non-zero reciprocal lattice vectors

$$\sum_{\boldsymbol{K}''} \gamma(\boldsymbol{K}, \boldsymbol{K}'', \omega)\varepsilon(\boldsymbol{K}'', \boldsymbol{K}', \omega) = \delta_{\boldsymbol{K}\boldsymbol{K}'}. \tag{38}$$

Note that both submatrices γ and ε are independent of the $\boldsymbol{q}$-vector. Using the explicit

expressions for the elements $\chi(\boldsymbol{q}, \boldsymbol{K}, \omega)$ and $\chi(\boldsymbol{K}, \boldsymbol{q}, \omega)$ as defined by equations (34) and (35), simple matrix manipulations yield the following results:

$$\chi^{-1}(0, 0, \omega) = (\chi(0, 0, \omega) - \tfrac{1}{3} \sum_{\boldsymbol{K}} \sum_{\boldsymbol{K}'} (\boldsymbol{K} \cdot \boldsymbol{K}')\sigma(0, \boldsymbol{K}, \omega)\gamma(\boldsymbol{K}, \boldsymbol{K}', \omega)\sigma(\boldsymbol{K}', 0, \omega))^{-1} \tag{39}$$

$$\chi^{-1}(0, \boldsymbol{K}, \omega) = -[(\boldsymbol{q} \cdot \boldsymbol{K})/|\boldsymbol{q}|]\tau(0, \boldsymbol{K}, \omega) \tag{40}$$

$$\chi^{-1}(\boldsymbol{K}, 0, \omega) = -[(\boldsymbol{q} \cdot \boldsymbol{K})/|\boldsymbol{q}|]\tau(\boldsymbol{K}, 0, \omega) \tag{41}$$

$$\chi^{-1}(\boldsymbol{K}, \boldsymbol{K}', \omega) = \gamma(\boldsymbol{K}, \boldsymbol{K}', \omega) + (\boldsymbol{q} \cdot \boldsymbol{K})(\boldsymbol{q} \cdot \boldsymbol{K}')/q^2 \, [\chi^{-1}(0, 0, \omega)]^{-1}\tau(\boldsymbol{K}, 0, \omega)\tau(0, \boldsymbol{K}', \omega). \tag{42}$$

Similar to $\sigma(0, \boldsymbol{K}, \omega)$ and $\sigma(\boldsymbol{K}, 0, \omega)$ the scalar functions $\tau(\boldsymbol{K}, 0, \omega)$ and $\tau(0, \boldsymbol{K}, \omega)$ are the same for each shell and are defined by

$$\boldsymbol{K}\tau(\boldsymbol{K}, 0, \omega) = \chi^{-1}(0, 0, \omega) \sum_{\boldsymbol{K}'} \gamma(\boldsymbol{K}, \boldsymbol{K}', \omega)\boldsymbol{K}'\sigma(\boldsymbol{K}', 0, \omega) \tag{43}$$

$$\boldsymbol{K}\tau(0, \boldsymbol{K}, \omega) = \chi^{-1}(0, 0, \omega) \sum_{\boldsymbol{K}'} \boldsymbol{K}'\sigma(0, \boldsymbol{K}', \omega)\gamma(\boldsymbol{K}', \boldsymbol{K}, \omega). \tag{44}$$

For nearly all frequencies the elements $\chi(0, 0, \omega)$ dominate all other elements with the consequence that, according to (39), $\chi^{-1}(0, 0, \omega)$ approximately coincides with the inverse of $\chi(0, 0, \omega)$ and is quite small. From equations (43) and (44) it follows that the scalar functions $\tau(\boldsymbol{K}, 0, \omega)$ and $\tau(0, \boldsymbol{K}, \omega)$ will also be small for nearly all frequencies. This is also true for the second term in equation (42) which causes the matrix elements $\chi^{-1}(\boldsymbol{K}, \boldsymbol{K}', \omega)$ to depend on the orientation of the wavevector $\boldsymbol{q}$ even in the case of the vanishing absolute value.

This general behaviour is confirmed by the numerical results which have been obtained by direct matrix inversion. To save space, only the frequency dependence of some characteristic elements of the inverse matrix $\chi^{-1}(\boldsymbol{q} + \boldsymbol{K}, \boldsymbol{q} + \boldsymbol{K}', \omega)$ are plotted.

Figure 9 shows a comparison of the element $\chi^{-1}(0, 0, \omega)$ with the reciprocal value of the element $\chi(0, 0, \omega)$ defined in the usual way as

$$1/\chi(0, 0, \omega) = [\chi_1(0, 0, \omega) - \mathrm{i}\chi_2(0, 0, \omega)]/[\chi_1^2(0, 0, \omega) + \chi_2^2(0, 0, \omega)]. \tag{45}$$

Over a wide range of frequencies, both curves coincide for the real as well as for the imaginary part. Even the greatest differences occurring in the frequency range 0.85 Ryd $\leq \omega \leq$ 1.6 Ryd and 2.0 Ryd $\leq \omega \leq$ 2.5 Ryd are less than 5%. These results explicitly confirm that in equation (39) the contribution due to the double sum is for most frequencies quite small with respect to $\chi(0, 0, \omega)$. Thus, local-field corrections have a slight influence on the macroscopic dielectric function in the long-wave limit. This justifies the comparison of the element $\chi(0, 0, \omega)$ with the experimental spectra $\chi(0, \omega)$ performed in section 6.1. As inclusion of exchange has no influence on $\chi(0, 0, \omega)$ the corresponding corrections are only expected in those regions where $\chi^{-1}(0, 0, \omega)$ differs from $1/\chi(0, 0, \omega)$. These corrections turned out to be up to 2%.

Figure 10 shows typical examples of diagonal elements of $\chi^{-1}(\boldsymbol{K}, \boldsymbol{K}, \omega)$ with non-zero reciprocal lattice vectors. The real part turns out to be close to 1.0 and to have a weak frequency dependence. In the frequency range considered, the imaginary part steadily increases with increasing frequency and possesses the peculiar structure at 1.75 Ryd common to all spectra. Inclusion of the exchange decreases the imaginary part by a factor of up to 1.6, whereas the real part is increased by less than 15%.

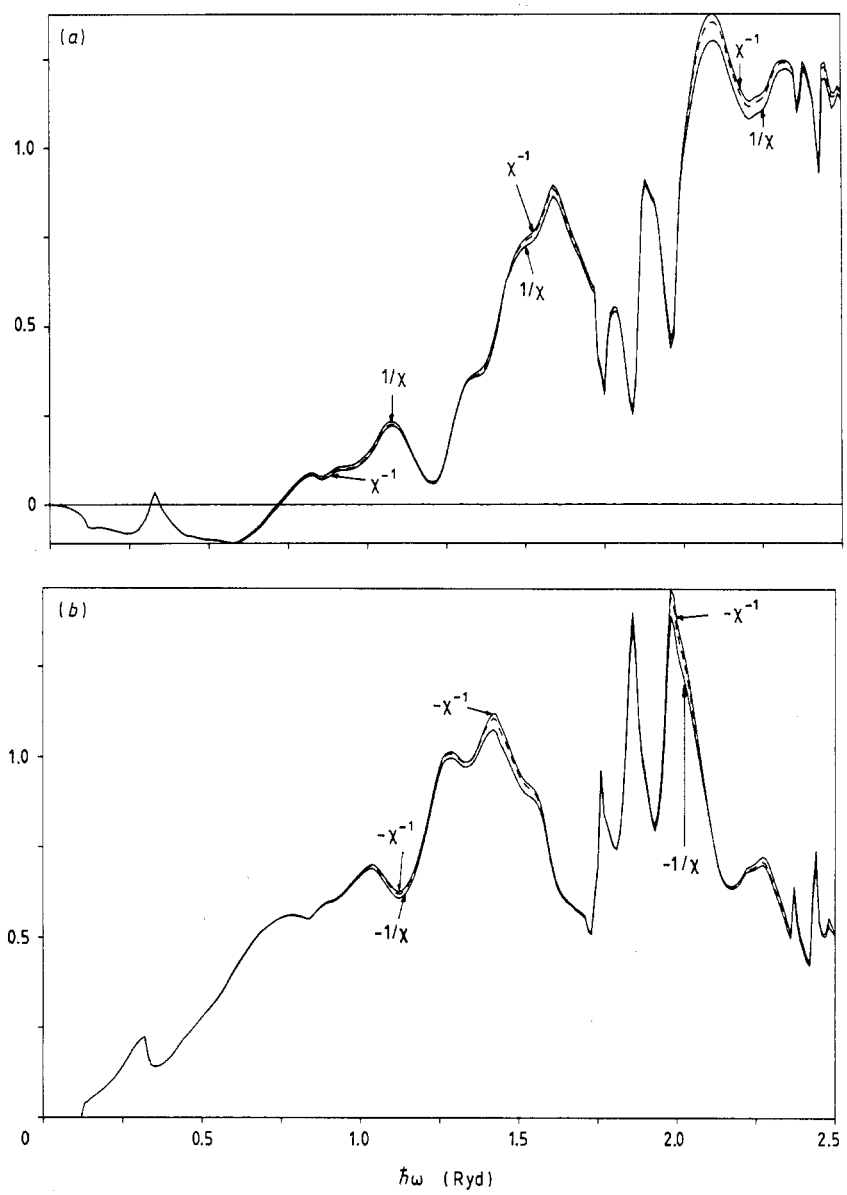

Figure 9. The dependence of the element $\chi^{-1}(0, 0, \omega)$ and of $1/\chi(0, 0, \omega)$ on the energy $\hbar\omega$(Ryd): (*a*) real part; (*b*) imaginary part. The broken curve incorporates the contribution due to exchange in $\chi^{-1}(0, 0, \omega)$.

According to equation (42) the diagonal elements with non-zero reciprocal lattice vectors should depend on the orientation of the $\boldsymbol{q}$-vector even in the long-wave limit. This is due to the functions $\tau(\boldsymbol{K}, 0, \omega)$ and $\tau(0, \boldsymbol{K}, \omega)$ which are found to be very small, apart from the region where $\chi^{-1}(0, 0, \omega)$ differs from $1/\chi(0, 0, \omega)$.

Again in figure 10 the reciprocal function of $\chi(\boldsymbol{K}, \boldsymbol{K}, \omega)$ defined analogously to equation (45) is plotted in order to demonstrate that in this case the local-field corrections are rather important. At low frequencies, we have found that the real part of $\chi^{-1}(\boldsymbol{K}, \boldsymbol{K}, \omega)$

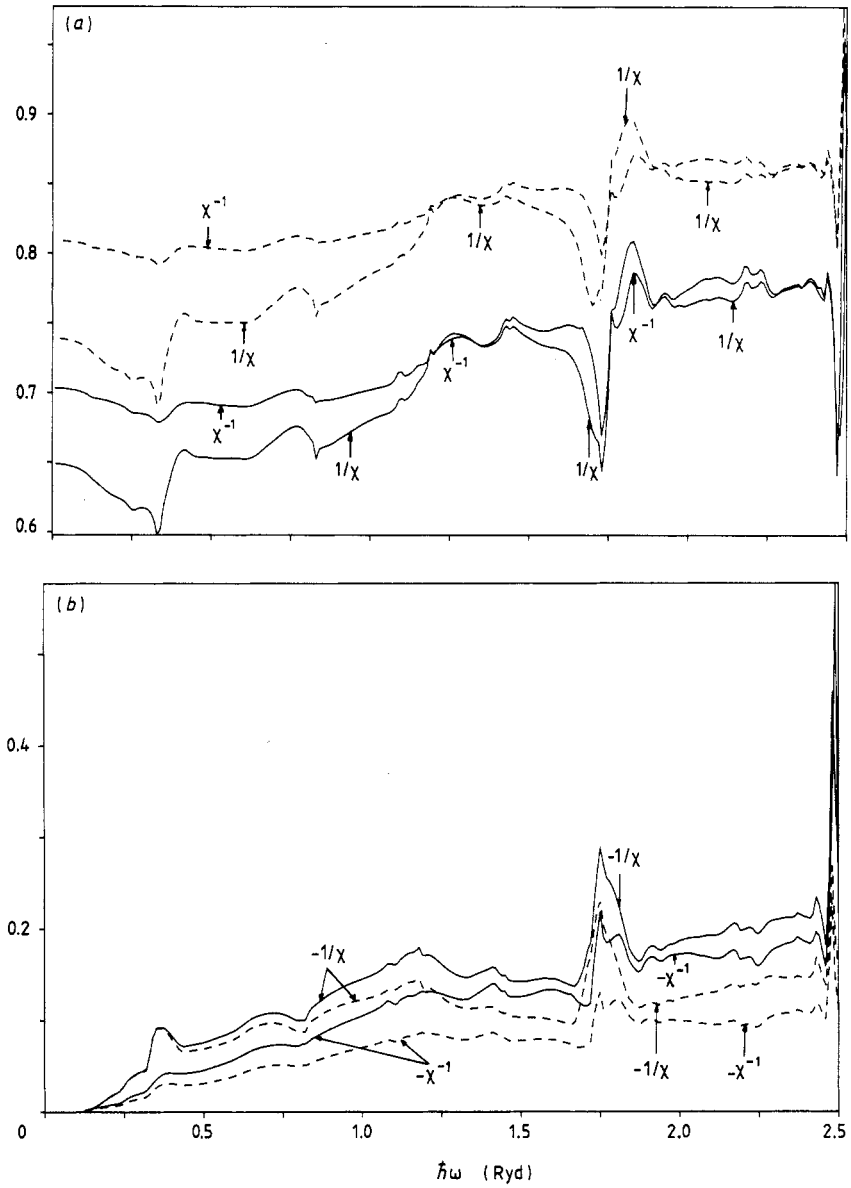

Figure 10. The dependence of the diagonal element $\chi^{-1}(\boldsymbol{K}, \boldsymbol{K}, \omega)$ and of $1/\chi(\boldsymbol{K}, \boldsymbol{K}, \omega)$ on the energy $\hbar\omega$(Ryd) with $\boldsymbol{K} = (2\pi/a)\ (1, 1, 1)$: (*a*) real part; (b) imaginary part. The broken curves incorporate the corresponding contributions due to exchange.

is approximately 12% larger than $[1/\chi(\boldsymbol{K}, \boldsymbol{K}, \omega)]_1$; with increasing frequency the difference becomes smaller and in the frequency range 1.5 Ryd $\leq \omega \leq$ 2.5 Ryd both curves come quite close. The value obtained in the static limit fits quite well with the results derived by Kubo [38]. For $\boldsymbol{q} = (2\pi/a)(0.5, 0.5, 0.5)$ the corresponding values for $\chi^{-1}(\boldsymbol{q}, \boldsymbol{q}, 0)$ and $1/\chi(\boldsymbol{q}, \boldsymbol{q}, 0)$ are 0.3867 and 0.3390, respectively. Local-field corrections have a still greater influence on the imaginary part. At low frequencies, $-[\chi^{-1}(\boldsymbol{K}, \boldsymbol{K}, \omega)]_2$

is a half and at a higher frequency two thirds of $-[1/\chi(\boldsymbol{K}, \boldsymbol{K}, \omega)]_2$. Thus, up to 1.25 Ryd the corrections due to exchange exceed those due to the local-field effects. Finally, we note that the inversion of the dielectric function causes a smoothing of the inverse function. Only those features which are common to all elements of the dielectric matrix will survive, e.g. the peak at 1.75 Ryd.

To save space, we would like to mention only that all non-diagonal elements are found to be by more than an order of magnitude smaller and, in most cases, more dependent on the frequency than are the diagonal elements. The influence of the inclusion of exchange is not unique. In some cases it yields a considerable increase and in other cases a decrease in the matrix elements $\chi^{-1}(\boldsymbol{K}, \boldsymbol{K}, \omega)$.

8. Conclusion and summary

The present paper has two major results. First, it demonstrates that the investigation based on band-structure results suffers from the fact that the real part of the dielectric function $\varepsilon(\boldsymbol{q}+\boldsymbol{K}, \boldsymbol{q}+\boldsymbol{K}', \omega)$ can be derived only with limited accuracy as the number of interband transitions to higher bands is limited. In the specific case where up to 70 eigenstates above the Fermi level have been considered, the accuracy for the diagonal elements has been found to be 20–30%. As the final energies ε_{nk} are restricted by the energy conservation $\varepsilon_{nk} \leqslant E_F + \hbar\omega$, these difficulties do not occur with the imaginary part and thus we expect it may be computed with higher accuracy. Second, as for most frequencies the element $\varepsilon(0, 0, \omega)$ dominates all other elements of the dielectric matrix, we have found in the long-wave limit that neither the local-field corrections nor many-body corrections which follow from the TLDF have a significant influence on the element $\varepsilon^{-1}(0, 0, \omega)$ of the inverse matrix. Therefore, the macroscopic dielectric function $\varepsilon(0, \omega)$ is well approximated by the element $\varepsilon(0, 0, \omega)$. As the incompleteness of the final state has a lesser influence on $\varepsilon_2(0, \omega)$ than on $\varepsilon_1(0, \omega)$, comparisons with experimental $\varepsilon_2(0, \omega)$ are more promising, provided that such information is available and not obscured, for example, by a Kramers–Kronig inversion of the experimental data.

For non-vanishing reciprocal lattice vectors the influence of the local-field corrections as well as the influence of many-body corrections are not negligible. The latter corrections are found to enforce the shielding over the whole frequency region, whereas the former yield a fractional decrease in the shielding at lower frequencies. Further investigations are desirable in order to decide whether it is appropriate to approximate the many-body effects by

$$\alpha_{xc}(\boldsymbol{q}+\boldsymbol{K}, \boldsymbol{q}+\boldsymbol{K}', \omega) \simeq (|\boldsymbol{q}+\boldsymbol{K}|^2/4\pi e^2) F(\boldsymbol{K}) \alpha_H(\boldsymbol{q}+\boldsymbol{K}, \boldsymbol{q}+\boldsymbol{K}', \omega) \tag{46}$$

where $F(\boldsymbol{K})$ is the Fourier coefficient of the leading spherical contribution of $\overline{\mathrm{d}V_{xc}}/\mathrm{d}\rho$.

Acknowledgments

O Belhachemi and B Mekki would like expressly to thank the German Exchange Service (DAAD) and A Seoud the Egyptian Government for their generous support.

References

[1] Adler S L 1962 *Phys. Rev.* **126** 413

[2] Bagayoko D, Laurent D G, Singhal S P and Callaway J 1980 *Phys. Lett.* **76A** 187
[3] Bailyn M 1960 *Phys. Rev.* **117** 974
[4] Baldereschi A 1973 *Phys. Rev.* B **7** 5212
[5] Bardeen J 1936 *Phys. Rev.* **50** 1098
[6] Beaglehole D, De Crescenti M, Thèye M L and Vuye G 1979 *Phys. Rev.* B **19** 6306
[7] Balhachemi O H 1986 *PhD Thesis* University of Munich, Federal Republic of Germany
[8] Bonch-Bruevich V L and Tyablikov S V 1962 *The Green Function Method in Statistical Mechanics* (Amsterdam: North-Holland) p 1
[9] Bross H 1964 *Phys. Kondens. Mater.* **3** 119
[10] Bross H 1968 *Helv. Phys. Acta* **41** 717
[11] Bross H and Hoffmann I 1969 *Z. Phys.* **229** 123
[12] Bross H, Bohn G, Meister G, Schubö W and Stöhr H 1970 *Phys. Rev.* B **2** 3098
[13] Bross H 1978 *J. Phys. F: Met. Phys.* **8** 2631
[14] Bross H and Eder R 1987 *Phys. Status Solidi* b **144** 175
[15] Bross H and Stryczek R A 1987 *Phys. Status Solidi* b **144** 675
[16] Bross H and Mekki B 1988 unpublished
[17] Chadi D J and Cohen M L 1973 *Phys. Rev.* B **8** 5747
[18] Chen A B 1976 *Phys. Rev.* B **14** 2384
[19] Dobson J F and Rose J H 1982 *J. Phys. C: Solid State Phys.* **15** 7429
[20] Eckard W 1985 *Phys. Rev.* B **31** 1985
[21] Ehrenreich H and Cohen M H 1959 *Phys. Rev.* **115** 786
[22] Ehrenreich H and Philipp H R 1962 *Phys. Rev.* **128** 1622
[23] Fetter L A and Walecka D 1971 *Quantum Theory of Many-Particle Systems* (New York: McGraw-Hill)
[24] Gupta R P and Sinha S K 1971 *Phys. Rev.* B **3** 2461
[25] Hagemann H J, Gudat W and Kunz C 1975 *J. Opt. Soc. Am.* **65** 742
[26] Hanke W R 1973 *Phys. Rev.* B **8** 4585
[27] Hedin L and Lundquist S 1969 *Solid State Physics* vol 23 ed F Seitz, D Turnbull and H Ehrenreich (New York: Academic) p 1
[28] Ho K M, Ihm J and Joannopoulos J D 1982 *Phys. Rev.* B **25** 4260
[29] Hohenberg P and Kohn W 1964 *Phys. Rev.* **136** B864
[30] Hone D 1960 *Phys. Rev.* **120** 1600
[31] Janak J F, Williams A R and Moruzzi V L 1975 *Phys. Rev.* B **11** 1522
[32] Johnson D L 1974 *Phys. Rev.* B **9** 4475
[33] Johnson P B and Christy R W 1972 *Phys. Rev.* B **6** 4370
[34] Johnson P B and Christy R W 1975 *Phys. Rev.* B **11** 1315
[35] Jones W and March N H 1973 *Theoretical Solid State Physics* (London: Wiley)
[36] Kohn W and Rostocker N 1954 *Phys. Rev.* **94** 1111
[37] Kohn W and Sham L J 1965 *Phys. Rev.* A **140** 1133
[38] Kubo Y 1976 *J. Phys. Soc. Japan* **40** 1339
[39] Kubo Y and Wakoh S 1981 *J. Phys. Soc. Japan* **50** 835
[40] Liebsch A 1985 *Phys. Rev.* B **32** 6255
[41] Mekki B 1986 *PhD Thesis* University of Munich, Federal Republic of Germany
[42] Monkhorst H J and Pack J D 1976 *Phys. Rev.* B **13** 5188
[43] Moruzzi V L, Williams A R and Janak J F 1978 *Calculated Electronic Properties of Metals* (New York: Pergamon)
[44] Persson M and Hellsing B 1984 *Phys. Rev.* B **29** 360
[45] Pick R M, Cohen M A and Martin R M 1970 *Phys. Rev.* B **1** 910
[46] Pines D 1964 *Elementary Excitations in Solids* (New York: Benjamin)
[47] Pines D and Nozières P 1966 *The Theory of Quantum Liquids* (New York: Benjamin)
[48] Seoud A E H 1983 *PhD Thesis* University of Munich, Federal Republic of Germany
[49] Slater J C 1937 *Phys. Rev.* **51** 846
[50] Stott M J and Zaremba E 1979 *Phys. Rev.* A **21** 12
[51] Uspenski Yu A, Maksimov E G, Rashkeev S N and Mazin I I 1983 *Z. Phys.* B **53** 263
[52] van Barth U and Hedin L 1972 *J. Phys. C: Solid State Phys.* **5** 1629
[53] Weber W 1988 *Diploma Thesis* University of Munich, Federal Republic of Germany
[54] Wiser N 1963 *Phys. Rev.* **129** 62
[55] Zangwill A and Soven P 1979 *Phys. Rev.* A **21** 1561